

Effects of the IDH1 R132H Mutation on the Energy Metabolism: A Comparison between Tissue and Corresponding Primary Glioma Cell Cultures

Lennard J. M. Dekker, Cassandra Verheul, Nicky Wensveen, William Leenders, Martine L. M. Lamfers, Sieger Leenstra, and Theo M. Luider*



Cite This: *ACS Omega* 2022, 7, 3568–3578



Read Online

ACCESS |



Metrics & More

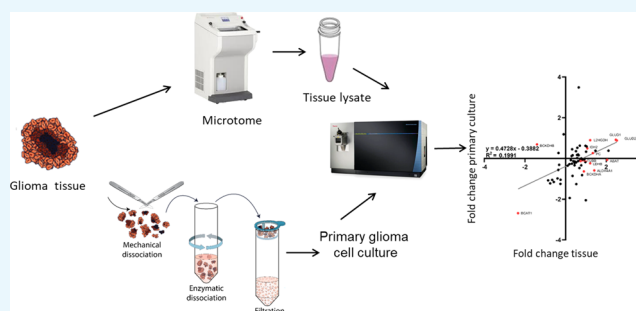


Article Recommendations



Supporting Information

ABSTRACT: The R132H mutation in the metabolic enzyme isocitrate dehydrogenase 1 (IDH1) is the most important prognostic factor for the survival of glioma patients. Subsequent studies led to the discovery of a panel of enzymes mainly involved in glutamate anaplerosis and aerobic glycolysis that change in abundance as a result of the *IDH1* mutation. To further study these changes, appropriate glioma models are required that accurately mimic *in vivo* metabolism. To investigate how metabolism is affected by *in vitro* cell culture, we here compared surgically obtained snap-frozen glioma tissues with their corresponding primary glioma cell culture models with a previously developed targeted mass spectrometry proteomic assay. We determined the relative abundance of a panel of metabolic enzymes. Results confirmed increased glutamate use and decreased aerobic glycolysis in resected IDH1 R132H glioma tissue samples. However, these metabolic profiles were not reflected in the paired glioma primary cell cultures. We suggest that culture conditions and tumor microenvironment play a crucial role in maintaining the *in vivo* metabolic situation in cell culture models. For this reason, new models that more closely resemble the *in vivo* microenvironment, such as three-dimensional cell co-cultures or organotypic multicellular spheroid models, need to be developed and investigated.



INTRODUCTION

Glioma is the most common malignant primary brain tumor and accounts for more than 80% of malignant primary brain tumors. Patients diagnosed with glioma have a poor prognosis with only about 20% of patients surviving 5 years after diagnosis, despite aggressive treatment with surgery, chemotherapy, and radiotherapy.¹ The mutation status of the gene encoding the *IDH1* enzyme is an important prognostic factor for patient survival. This mutation occurs early in gliomagenesis and is very common in low-grade gliomas (WHO grades II and III) and grade IV gliomas that have progressed from lower grades (secondary glioblastomas).² Patients diagnosed with a secondary glioblastoma carrying the IDH1-R132H mutation (IDH1 mut) have a better prognosis than patients with a primary glioblastoma with the wild-type (wt) *IDH1* gene (31 versus 15 months overall survival).³

The IDH1 enzyme is active in the cytoplasm and converts isocitrate into α -ketoglutarate (α -KG), producing NADPH. IDH1 R132H (IDH mut) however converts α -KG into the oncometabolite D-2-hydroxyglutarate.⁴ Importantly, during this process, NADPH is oxidized to NADP⁺, which results in oxidative stress.⁵ Previously, we and others studied the effects of this mutation by analyzing the transcriptome, proteome, and metabolome of tumor tissue samples with and without the

mutation.^{6–10} We observed that this mutation leads to metabolic changes in the tumor where the import of both glutamate and lactate, rather than glucose, is increased to fuel the tricarboxylic acid (TCA) cycle.^{6,7} This metabolic adaptation probably compensates for decreased NADPH levels and provides α -KG as a TCA cycle substrate.^{11,12} Blocking of glutamate dehydrogenase, which converts glutamate to α -KG, by the green tea catechol epigallocatechin gallate (EGCG) resulted in decreased tumor cell proliferation and increased sensitivity to radiotherapy in HCT116 colorectal cancer cells with a knock in *IDH1* mutant gene compared to control lines.¹³

IDH1 mutant glioma models are crucial to test new treatment concepts for this now incurable disease. Unfortunately, such models are notoriously difficult to establish and are only available to a limited extent.¹⁰ This complicates *in*

Received: November 1, 2021

Accepted: December 24, 2021

Published: January 19, 2022



in vitro studies of the effects of the IDH1 mut in glioma tissues. A glioma xenograft model in mice with endogenous IDH1 mutation was shown to have characteristics similar to clinical IDH1-R132H gliomas.⁷ This model could potentially be useful, but there are practical limitations. In particular, high-throughput compound screening experiments are not feasible. In our laboratory, a culturing procedure has been developed to reliably obtain primary glioma cultures from glioma tissues, also with the IDH1 mut.¹⁴ We showed that the IDH1 mutation is retained in a set of 12 patient-derived glioma cultures. These cultures can easily be used in drug screening experiments.¹⁵ However, to confirm that these cultures are a suitable model for the energy metabolism in clinical glioma, especially for therapeutic interventions focused on the disruption of metabolic pathways, the metabolic profiles of the cell cultures need to be compared with those of the corresponding glioma tissues.

In this study, a set of primary glioma cell cultures along with the corresponding clinical tissues was analyzed using proteomics. Since most of the successful cultures with the mutation are high-grade gliomas (secondary glioblastomas), a comparison of low-grade and high-grade glioma tissues was included to determine the influence of tumor grade. We utilized our previously developed targeted mass spectrometry assay to obtain a relative quantitative measure of the protein abundance for a panel of metabolic enzymes involved in aerobic glycolysis, amino acid catabolism, fatty acid metabolism, glutaminolysis, glycolysis, pentose phosphate pathway, and TCA cycle. In addition, we present a targeted mass spectrometry assay that can be used to confirm and quantify the presence of the IDH1 mutation in the used cell cultures and tissues.

RESULTS

From the previously described panel⁶ of metabolic enzymes involved in aerobic glycolysis, amino acid catabolism, fatty acid metabolism, glutaminolysis, glycolysis, pentose phosphate pathway, and TCA cycle, all 64 proteins could be detected in the cohort of glioma tissue samples analyzed in the current study (Table 1). This panel consists of 120 peptides corresponding to the 64 proteins, of which 8 proteins were measured with one peptide and 56 with two peptides. For the primary cell cultures, the peptides corresponding to the proteins SLC16A3 and SLC16A7 were below the detection

Table 1. Tissues and Corresponding Cultures Sample Information^a

groups	grade	average patient age (min–max)
IDH1 R132H mutation (total: <i>n</i> = 27; <i>n</i> = 6)	II–IV	36.1 (21–67), 40.0 (25–58)
astrocytoma (<i>n</i> = 8; <i>n</i> = 1)	II	41.2 (25–67), 36 (25–47)
anaplastic astrocytoma (<i>n</i> = 9; <i>n</i> = 1)	III	31.3 (21–44), 38
secondary glioblastoma (<i>n</i> = 9; <i>n</i> = 4)	IV	35.8 (21–58), 38.8 (25–58)
IDH1 wild type		
glioblastoma (<i>n</i> = 8; <i>n</i> = 5)	IV	57.6 (44–66), 60.4 (56–66)

^aNote: Numbers within parentheses indicate the total number of tissue samples, and the numbers indicate the number of tissue samples with a corresponding primary cell culture.

limit. For this reason, both proteins were removed from the further analyses of primary cell culture data. This resulted in a panel consisting of 116 peptides, which corresponds to 62 proteins.

We compared IDH1 wt tissues with the IDH1 mut tissues of all grades combined. The results of this analysis are visualized in a volcano plot (Figure 1), which shows that 21 of the

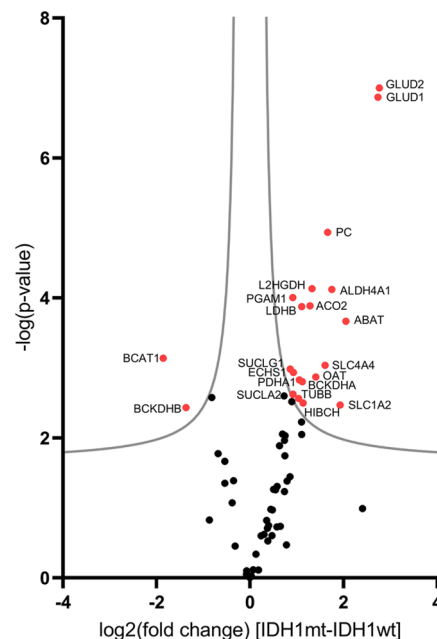


Figure 1. Volcano plot comparing the IDH1 mut tissue group with the IDH1 wt tissue group. The plot shows the \log_2 (fold change) as a function of the $-\log(p\text{-value})$ for each protein. The groups consist of 8 IDH1 wt samples and 27 IDH1 mut samples. The gray line indicates the significance threshold and is defined by an s_0 of 0.1 (\log_2 (fold change) threshold of 0.1) and an FDR of 0.05 ($-\log p\text{-value}$ threshold). All proteins above this threshold are significantly different between the IDH1 mut and the IDH1 wt group. The significant proteins are labeled with their gene name and are shown in red.

selected proteins have statistically significant fold changes between the IDH1 mut and the IDH1 wt group (FDR 5%). The majority of these proteins (19 proteins) were upregulated in the IDH1 mut tumors, while two proteins were downregulated. A complete overview of all p -values and fold changes is shown in Supporting Information Table S4. Twenty of the significant proteins are involved in one of the studied metabolic pathways. Six proteins function in the TCA cycle, seven in the glutaminolysis, one in the glycolysis, two in the aerobic glycolysis, one in the lipid metabolism, and three in the amino acid catabolism. The proteins involved in glutaminolysis show the highest fold changes. Supporting Information Figure S1 shows a correlation plot, comparing the \log_2 fold changes of the current study to those found in the previous study for the 64 overlapping proteins. These fold changes correlate ($R^2 = 0.56$) with the fold changes found in the previous study.⁶

The IDH1 mut culture group contains a higher number of high-grade (IV) glioma tumors (secondary GBM) compared to the IDH1 wt tissue group. For this reason, the influence of this factor was investigated. To determine the effect of tumor grade on the differences observed for the metabolic panel, low-grade IDH1 mut astrocytomas (grade II) and high-grade IDH1

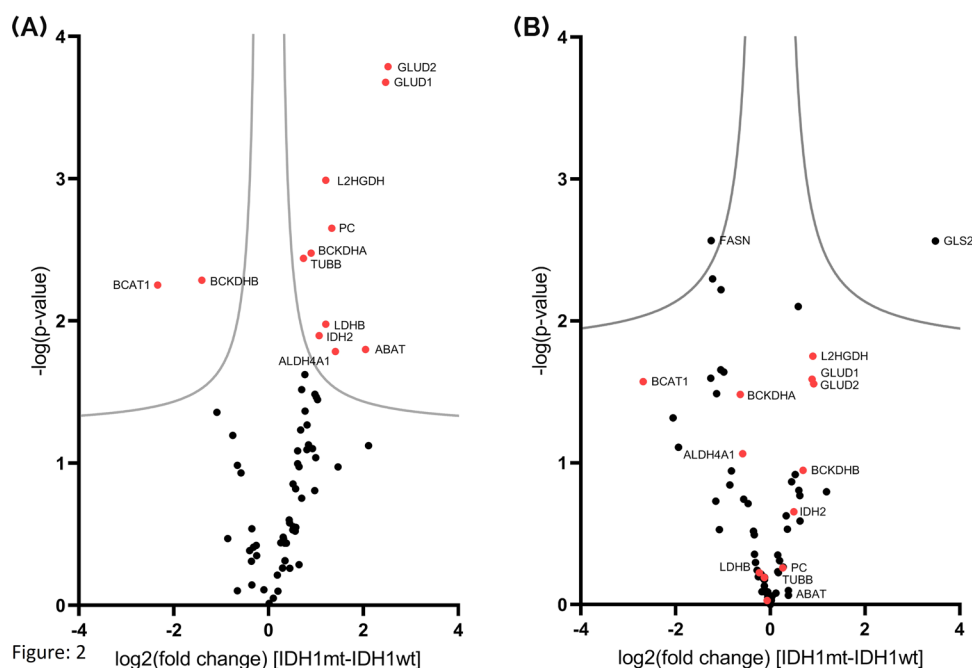


Figure 2. Volcano plot comparing the IDH1 mut group with the IDH1 wt group for both the tissue subset (A) and the corresponding cultures (B). The plots show the \log_2 (fold change) as a function of the $-\log(p\text{-value})$ for each protein. The analyzed samples are a subset of the tissues samples for which corresponding cultures were available (A) and the corresponding cultures (B). The groups consist of six IDH1 mut samples and five IDH1 wild-type samples. The gray lines indicate the threshold for statistical significance between IDH1 mut and IDH1 wt and are defined by an s_0 of 0.1 and an FDR of 0.05. All proteins above this threshold are significantly different between the IDH1 mut and the IDH1 wild-type group. (A) Differences between the IDH1 mut and IDH1 wild-type tissue samples. All significantly different proteins are labeled with their gene name and are shown in red. (B) Differences between the IDH1 mut and IDH1 wild-type culture samples. All significantly different proteins in the tissues are shown in red. Proteins FASN and GLS2 are found to be significantly different between the IDH1 mut and IDH1 wt glioma cell cultures.

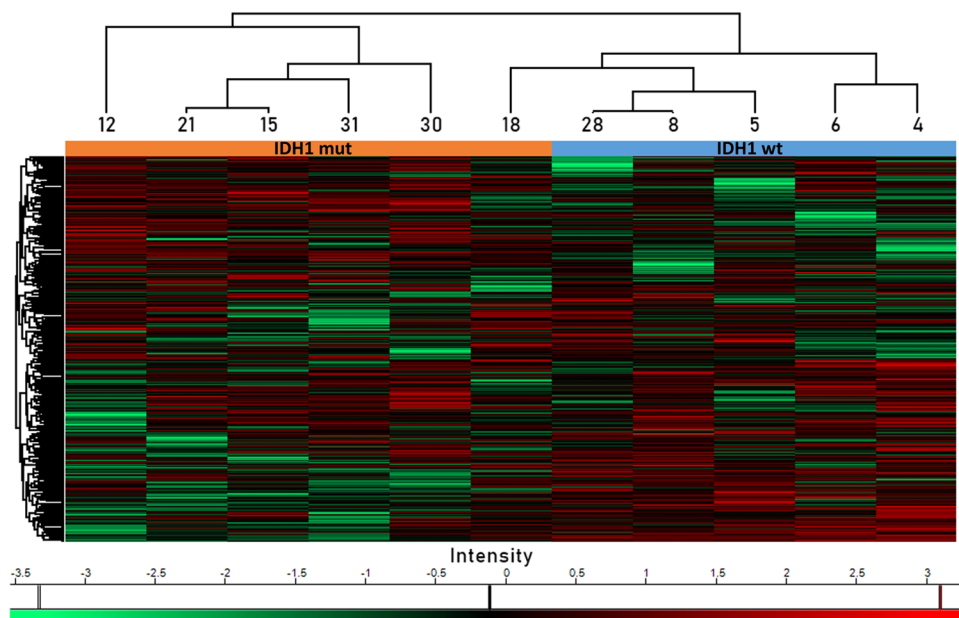


Figure 3. Clustering heat map of 11 primary glioma culture samples based on z -score normalized spectral counts. A total of 4247 protein groups were used in this clustering. The different samples are clustered horizontally, and the different proteins are clustered vertically. The IDH1 mut sample cluster separates from the IDH1 wt samples. However, one of the IDH1 wt samples clusters with the IDH1 mut samples.

mut secondary glioblastomas (grade IV) were compared. The result of this analysis is depicted in the volcano plot in Supporting Information Figure S2. None of the metabolic enzymes were statistically significantly different between the low-grade and high-grade glioma group, indicating that the

influence of tumor grade on the abundance of the enzymes in the metabolic panel is very limited (Figure S2).

The same panel of metabolic enzymes was also applied to 11 primary glioma cell culture samples, derived from a subset of the tissue samples (see Table 1). To allow justified comparisons, a separate analysis was performed on this subset

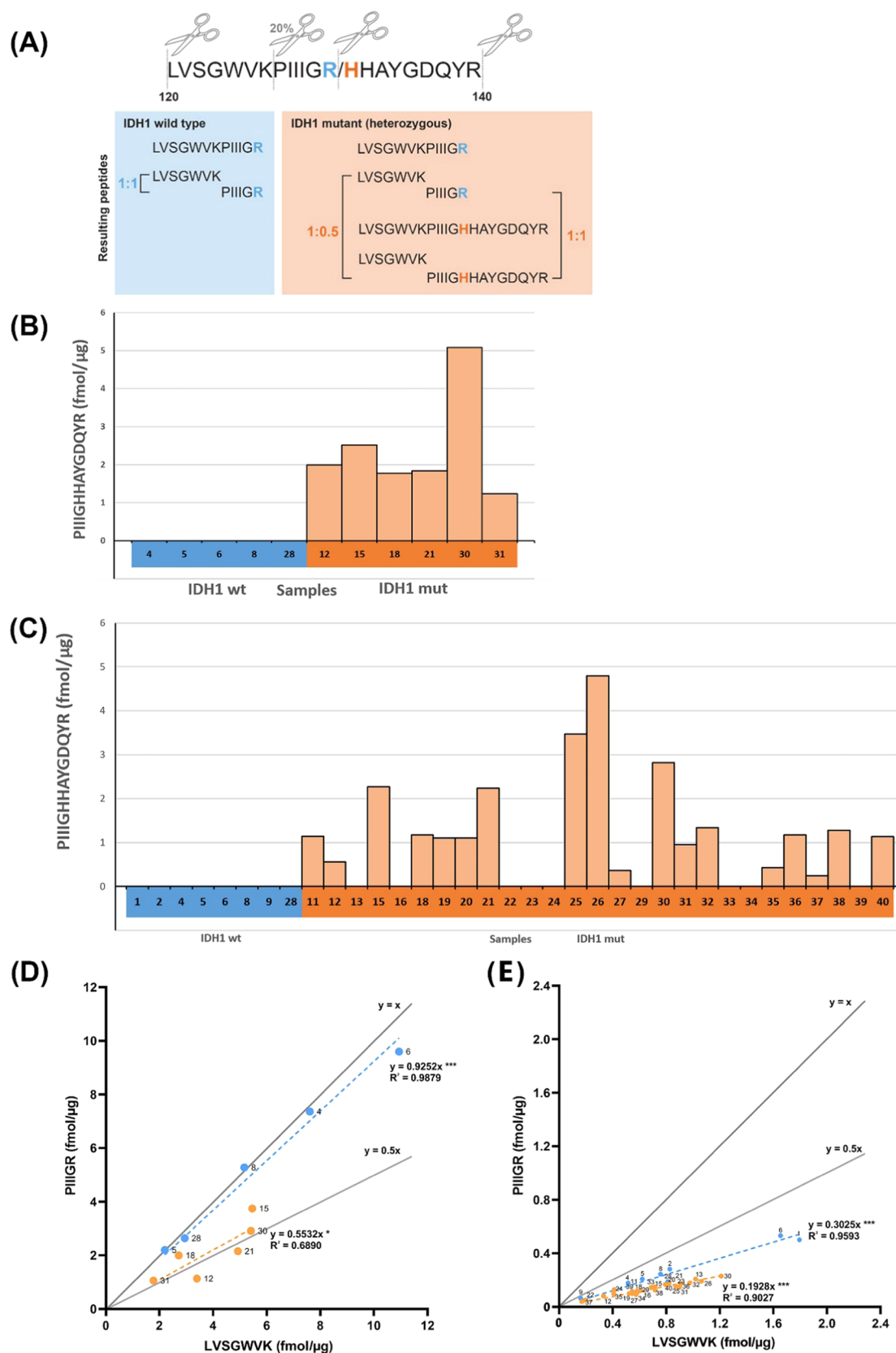


Figure 4. Quantification of IDH1 R132H mutation in glioma tissues and primary cell cultures. (A) Wild-type peptide “LVSGWVKPIIIGR” contains a proline right after the trypsin cleavage site (cleaves after arginine (R) and lysine (K)) and is therefore only cleaved in about 20% of cases. Therefore, the formation of the LVSGWVK and PIIIGR peptide is rate-limited by the trypsin cleavage of this site. IDH1-R132H is a heterozygous mutation, which should result in the formation of both wild-type and R132H mutated IDH1 specific peptides. The amount of IDH1 wild-type peptides is therefore expected to be lower in the IDH1 mut samples compared to the IDH1 wild-type samples. (B, C) Peptide concentration for mutant peptide PIIIGHAYGDQYR in the culture (B) and tissue (C) samples. On the *x*-axis, the different culture/tissue samples are shown, on

Figure 4. continued

the *y*-axis, the amount of the mutant peptide measured is shown in fmol/ μ g total protein content. (B) In the 5 IDH1 wt samples, the mutant-specific peptide is not detected. In the 6 IDH1 mut samples, this peptide is detected, which corresponds to the mutational status of the cultures. (C) In the 8 IDH1 wt samples, this mutant peptide is not detected. In the 27 IDH1 mut samples, this peptide is detected in 18 out of 27 samples. (D, E) Correlation of the peptides formed by cleavage of LVSGWVKPIIIGR in fmol/ μ g total protein in culture and tissue samples. Every dot represents a sample of one glioma culture or tissue. The blue dots are IDH1 wild-type cultures or tissues, and the orange dots are the IDH1 mut samples. The theoretical one-to-one ratio of these peptides is shown with the dark gray line; this is the expected ratio for the wild-type samples. If the wild-type and mutant IDH1 gene are co-dominant, the theoretical ratio of these peptides would be one to a half for the heterozygous mutation. This ratio is shown with the light gray line. (D) Cultures show a moderate correlation (0.6890) between peptides specific for the mutation site and the common peptides of IDH1 in IDH1 mut cultures and an excellent correlation (0.9879) between wild-type specific and the common IDH1 peptides. The difference in the ratio of these two peptides between the IDH1 wild-type group and the IDH1 mut group is seen in the slope of the lines. These values 0.9252 and 0.5532 are very near to that expected theoretically, 1 (IDH1 wt) and 0.5 (IDH1 mut), respectively. (E) There is a good correlation (0.9027) between peptides specific for the mutation site and the common peptide of IDH1 in the IDH1 mut tissues and an excellent correlation (0.9593) between wild-type specific and the common IDH1 peptides in the IDH1 wild-type tissues.

of tissue samples (six IDH1 mut and five IDH1 wt). For both the tissues (Figure 2A) and the cultures (Figure 2B), the volcano plots are shown. Complete overviews of all *p*-values and fold changes are listed in Supporting Information Table S5 (tissue subset) and Supporting Information Table S6 (cultures). All 21 proteins with a significantly altered fold change in the complete tissue set had the same direction of fold change as the subset. Of these proteins, 10 have a significantly altered fold change in the subset. In addition, two proteins that were not significant in the complete tissue set are significant in the subset. These proteins too show the same direction in fold change in the complete tissue set and the subset. A strong correlation of the tissue subset and the complete tissue set is present in Supporting Information (Figure S3). Comparing the IDH1 mut and IDH1 wt primary cell cultures, there were fewer significant changes in comparison with the tissue set, only FASN and GLS2 are significantly altered (above FDR threshold of 0.05) but do not overlap with the tissue. In addition, the directions of the fold changes of many proteins are different compared to those of the tissue subset. Most of the significant proteins in the tissue subset show only minor fold changes (between 0.6 and 1.6) in the cell cultures. Only BCAT, GLUD1/2, and L2HGDH show larger fold changes that are in the same direction as in tissue. Overall, this results in a limited correlation between the fold changes observed in the cultures and in the tissue subset (Supporting Information Figure S4).

In addition to the metabolic panel, a proteome-wide analysis was performed on the primary cell cultures as well. This resulted in the identification of 4247 proteins. On this data set, we used a cluster analysis (Figure 3). This analysis revealed that based on this unsupervised clustering two distinct sample clusters could be observed, one containing all of the IDH1 mut samples and the other all but one of the IDH1 wt samples. This shows that even though limited significant changes were observed in the metabolic panel, the proteome as a whole is quite different between the two sample groups. A further description of the differences between the IDH1 wt and IDH1 mut primary cell cultures is published by Verheul et al.¹⁴

To confirm the IDH1 mutation in the samples, a PRM analysis was performed using several peptides from IDH1, including peptides with and without the mutation. The IDH1 mutation changes the arginine (R) on the wild-type "PIIIGR" peptide of which the equivalent in the IDH1 R132H mutated form is peptide "PIIIGHHAYGDQYR" (Figure 4). The IDH1 mt peptide PIIIGHHAYGDQYR was picked up in all IDH1 mutated cell cultures and in none of the IDH1 wild-type cultures (Figure 4B). The IDH1 wt specific peptides were

detected in all cultures. We observed that the IDH1 mut cultures only have half of the amount of the wild-type specific IDH1 peptide PIIIGR compared to the peptide "LVSGWVK" that is present in both the wild-type and mutated IDH1 (Figure 4D). In tissue samples, the same panel of IDH1 peptides was more difficult to detect. The peptide PIIIGHHAYGDQYR, which is specific for the IDH1 mut proteins, is not detected in any of the IDH1 wild-type samples, nor in 9 out of the 27 IDH1 mut samples (Figure 4C). In the remaining 18 samples, a correlation between the common peptide LVSGWVK and IDH1 wt specific peptide PIIIGR for the tissue samples is still observed (Figure 4E). The difference in the ratio of the two peptides between the IDH1 wild-type group and the IDH1 mut group is reflected in the slope of the lines. The slopes are 0.3025 (IDH1 wt) and 0.1928 (IDH1 mut), which deviate from the theoretical value of 1 (IDH1 wt) and 0.5 (IDH1 mut).

Targeted transcriptome analyses previously showed that orthotopic xenograft mouse models E434 (IDH1 wt) and E478 (IDH1 R132H) had comparable metabolic profiles as clinical IDH1 wt and IDH1 mut glioma tissue samples.⁷ We reanalyzed the data sets for these xenografts and compared the differentially expressed genes to the differential proteome. We found that 40 genes of the targeted transcriptomics panel overlap with the proteomics panel (64 proteins). In Table S7, the fold changes of the tissues (27 IDH1 mut vs 8 IDH1 wt) and the xenografts (1 IDH1 mut vs 1 IDH1 wt) are compared. For most proteins (30 out of 40), the same fold change direction (up- or downregulated) is observed in the xenografts compared to the tissues. For 10 out of 11 significantly different proteins, the direction of fold change was also identical. In addition, the xenografts showed larger fold changes for these metabolic proteins in comparison to the cultures. A correlation plot comparing the xenografts to the complete tissue set can be observed in Supporting Information Figure S5.

DISCUSSION

The primary goal of this study was to assess whether differences in metabolic enzyme levels between IDH1 mutant and IDH1 wild-type gliomas are retained in culture. We previously found that large changes in protein abundances were observed for metabolic enzymes in pathways of aerobic glycolysis and glutaminolysis in IDH1 mutant gliomas. These changes may represent a survival mechanism of these tumors to keep the TCA cycle active and to ensure that sufficient NADPH is produced to accommodate fatty acid and membrane synthesis, an absolute requirement for tumor cell

growth.^{6,7,10} In this study, we investigated a more heterogeneous population of glioma tumor tissues that also includes high-grade *IDH1* mut tumors. In addition, primary cell cultures with and without the *IDH1* mut, derived from these clinical tumors, were analyzed. The results of this independent tissue data set are largely comparable with the previous study.⁶ The 21 significantly changed proteins in the current study fully overlap with the 48 significantly changed proteins in the previous study. Only two proteins, PGD and BCKDHB, were discordant with our previous study, showing a different fold change direction. The lower overall number of differentially expressed proteins is related to the smaller group size of the *IDH1* wt samples, which results in a lower statistical power (19 versus 8 samples).¹⁶ These results show that the data are reproducible and can be validated in an external tissue set.

With respect to the previous data set, one factor existed that may have caused a bias, which is the tumor grade. The *IDH1* mut culture group contained more high-grade (IV) glioma tumors (secondary GBM) compared to the *IDH1* mut tissue group. High-grade *IDH1* mut gliomas (secondary GBM) were overrepresented in our cohort of primary cell cultures, as the success rate of establishing cultures of low-grade gliomas is very low.^{17–20} For this reason, we investigated if tumor grade influences the abundance of the metabolic enzymes in the analyzed metabolic panel. The correlation between the previous and the current study ($R^2 = 0.56$) showed that tumor grade has no significant effect on the abundance of the metabolic enzymes investigated.

We could not establish primary cell cultures from all tumor samples. For this reason, matched tissue samples and cultures ($n = 11$) were analyzed separately. This analysis showed similar fold changes between *IDH* mut and *IDH* wt, as was observed in the complete tissue set ($n = 35$), showing that this subset was representative for the entire cohort. The p -value of the changed proteins tended to be lower in the subset, which is related to the smaller sample size.¹⁶ However, the analysis of the enzymes related to energy metabolism in the cell cultures revealed that the abundance poorly correlated with that of the matching tissue samples. The comparison of *IDH1* mut to *IDH1* wt cell cultures only results in two significantly different proteins (*FASN* and *GLS2*), which do not overlap with the tissue data. In addition, the fold changes, although non-significant, were often in the opposite direction of that observed in tissue. Proteins with the same fold change direction had in general a lower fold change compared to the tissue subset. During characterization of the glioma cultures, a similar observation was made at the RNA level.¹⁴ In this characterization study, RNAseq results showed minimal changes between *IDH1* wt and *IDH1* mut cultures for the genes related to the proteins in our metabolic proteomics panel. In addition, a correlation between the RNAseq and proteomics data was observed.

We and others previously showed that mutations in proteins in both cell cultures and tissues could be detected by mass spectrometry, including the *IDH1* mutation, but for these measurements, an enrichment by immunoprecipitation of the mutated protein was required.^{21,22} In the current study, we show that using the newest-generation mass spectrometry equipment, this step can be omitted. Using this assay, the *IDH1* mutation could be confirmed in all *IDH1* mut cultures and most of the tissues. The ratio of *IDH1* mut peptides to *IDH1* wt peptides was approximately 1:1 for the *IDH1* mut culture samples. This confirms that the *IDH1* mutation is

present in all cell cultures and that all cells in the cultures harbor a heterozygous *IDH1* mutation. However, in tissues, the *IDH1* status could not be confirmed in all samples with a mass spectrometry approach because the peptide containing the mutation could not be detected in all samples. In addition, the slopes do not show an exact ratio of 1:0.5 (*IDH1* wt/*IDH1* mut). This could be expected because the percentage of tumor cells in tissue is lower. This is also indicated by the correlation of tumor percentage and the ratio of *IDH1* mut to *IDH1* wt peptides. Despite potentially lower tumor percentages in these tissue samples, the effects of the *IDH* mutation could be clearly observed in our metabolic proteomics panel, indicating that probably the metabolic effects of the mutation extend beyond the tumor cells. However, quite a few deviations between tumor percentage and the ratio of *IDH1* mut to *IDH1* wt peptides are present, which could relate to a number of factors including the imprecision of proteomics analyses (measurements close to the detection limit); the effect of necrotic parts in the tumor (lower protein content but represent a substantial area); tumor areas containing a higher percentage of astrocytes, epithelial cells, immune cell infiltrates, microglia, and neuronal cells; and the presence of high abundant extracellular matrix proteins resulting in a lower overall signal and more background.²³

The confirmation of the *IDH1* mutation in the cell cultures does not explain the discrepancy between the cultures and tissues for the selected metabolic panel. It is reported in the literature that cell cultures are not an ideal model to study energy metabolism since a cell culture does not serve as an accurate representation of the *in vivo* situation.^{24–27} Potential deviating factors could be the culturing conditions (glucose and glutamate/glutamine concentrations in culture media, O_2 , and CO_2 pressure).²⁸ Modified culture conditions (lower glucose) that better represent the *in vivo* situation were tested but resulted in cell death. This showed that physiological glucose concentrations in the human brain²⁹ could not be reached under the current culture conditions. This is possibly caused by the use of standard high-glucose medium while establishing the cultures that could have resulted in cell selection or metabolic reprogramming. Another important difference between cell cultures and tumor tissues is the presence of nontumor cells in the tumor microenvironment (neuronal cells, astrocytes, epithelial cells, immune cells) and the extracellular matrix. It has been shown that the microenvironment plays an important role, as neurons and astrocytes are key players in the glutamine-glutamate cycle and lactate production, ensuring a state of metabolic homeostasis.⁷ An interaction between neurons and glioma tumor cells with the *IDH1* mut has been proposed by Lenting et al. to have a profound effect on energy metabolism in cultured cells.²⁴ Moreover, the concept of cancer stem cells proposes the presence of a small population of self-renewing cells that are tumor-initiating when injected in mice, and most likely responsible for therapy resistance in patients.³⁰ Culture conditions are known to enrich for tumor stemlike cells.³¹ Thus, it is hypothesized that *IDH* mutant glioma cells significantly interact with their surroundings creating a metabolically distinct environment, which may not be detected in pure tumor cell cultures. Previously, metabolic assays using the Seahorse system did reveal a difference in energy metabolism between the *IDH1* wt and mut primary cultures, with *IDH* mut having a lower mitochondrial reserve capacity.¹⁴ This could indicate that metabolic differences related to the

IDH1 mutation are still present in primary cultures but only to a limited extent and are possibly suppressed by, for instance, the culture conditions or absence of tumor microenvironment. Further Seahorse studies with tissue samples derived from IDH1 wt and IDH1 mut tumors are required to understand and validate this observation.

When the complete proteome of the cell cultures is considered, significant differences exist between the IDH1 mut and IDH1 wt primary cell cultures. In an unsupervised clustering analysis of the proteome-wide data, two main clusters exist that almost completely separate the IDH1 wt from the IDH1 mut cell culture samples. This indicates that a considerable number of proteins, other than the metabolic enzymes studied here, differentiate the two sample groups. These results are confirmed on the gene level where many genes besides the metabolic panel show a differential expression between IDH1 wt and mut cultures.¹⁴ These differences could be of potential interest to understand the effects of the IDH1 mutation on other cellular processes.

The number of studies investigating metabolic changes in glioma IDH1 mut models is limited. This is due to the low success rate of establishing IDH1 mut glioma models, which is associated with a lower growth rate of the IDH1 mut tumor *in vivo*.^{3,32} However, Lenting and co-workers presented a successful IDH1 mut xenograft model. Based on *in vivo* MRSI data of this xenograft mouse model, a lower lactate concentration was observed in the IDH1 mut compared to the IDH1 wild type. This is in line with the low LDHA-to-LDHB ratio that was observed on the RNA level in the IDH1 mut xenograft model. This lower ratio of LDHA to LDHB was also observed in the glioma tissue samples analyzed in this study and our previous study. Therefore, we compared the targeted RNA sequencing data of the two xenograft models (E434 IDH1 wt and E478 IDH1 mut) with our proteomics data.⁷ This comparison was performed on 40 genes that overlapped between protein panel (64) and the targeted gene panel (104). No statistical analysis could be performed on these overlapping genes since there is only one IDH1 mut xenograft model. The fold changes that were observed for these 40 genes between the xenografts indicate that the metabolism in these models significantly differs. Metabolic profiles of these models overlap with those in tissues although differences between the xenografts and clinical tumors still exist. A complicating factor is the unavailability of additional IDH1 mut xenograft models, so a validation of these results is at the moment not possible. Nevertheless, these results are a first indication that models that better represent the *in vivo* situation for the energy metabolism can be established. For this reason, co-cultures of IDH mutant cells with astrocytes and/or primary neurons, organotypic multicellular spheroids (OMS), or organotypic multicellular slices that are cultured from larger fragments of IDH1 mut gliomas are of interest.^{33,34} Current glioma culture protocols are aimed at maximizing the expansion of glioma stemlike cells. Ideally, levels and local concentrations of metabolites mimic the *in situ* conditions. IDH mutant gliomas are relatively slow-growing primary central nervous system tumors. To mimic the tumor behavior within a patient, nutrient levels should likely be reduced. Special culture plates that have continuous flow through their chambers or culture medium that is continuously swirled around could be considered.^{35,36} With so many options, and the notion that these tumors are so notoriously difficult to culture, finding the right conditions may be a challenge. It remains to be seen if

such models also recapitulate clinical tumors metabolically, as the presence of a functioning brain microenvironment is a potentially crucial factor.³⁷

In conclusion, we have confirmed our previous finding in an external data set and showed that the IDH1 mutation changes the energy metabolism independent of the tumor grade of the patient. In addition, the data shows that the studied panel of metabolic enzymes in IDH1 mut and IDH1 wt primary cell cultures is distinct from the corresponding glioma tissues. Primary glioma cell cultures, cultured under the current conditions, are for this reason not a suitable model for the part of the energy metabolism investigated in this study. In developing suitable culture conditions, a close resemblance to tumor microenvironment is crucial. The investigated IDH1 xenograft model partially overlaps with the *in vivo* situation, indicating that models can potentially be developed to resemble the patient situation more in energy metabolism. However, further research is required to confirm these observations due to the low sample number. The development of well-defined models is a key requirement to get information about how to therapeutically intervene with this disease.

MATERIALS AND METHODS

All chemicals were purchased from Sigma-Aldrich (Saint Louis, MO), and all solvents used for digestion/liquid chromatography–mass spectrometry (LC–MS) were purchased from Bio Solve (Valkenswaard, The Netherlands). The medium and added supplements used for the cell cultures were purchased from Thermo Fisher Scientific (Invitrogen, Gibco, or Alfa Aesar) unless otherwise noted.

Samples. A total of 35 fresh frozen tissue samples of surgically resected gliomas from 35 patients were analyzed. From 11 tissue samples, the corresponding primary glioma cell cultures were established. The gliomas were classified based on the guidelines provided by the World Health Organization (WHO, 2016).³⁸ The set consisted of eight diffuse astrocytomas (grade II; IDH1 mut), nine anaplastic astrocytomas (AA) (grade III; IDH1 mut), nine secondary glioblastomas (grade IV; IDH1 mut), and eight glioblastomas IDH1 wild type (IDH1 wt). Additional information is shown in Tables 1 and S1. Characteristics of the 11 matching primary glioma cell cultures (6 IDH1 mut, 5 IDH1 wt) are shown in red in Table 1. The use of patient material was approved by the Institutional Review Board of the Erasmus MC, Rotterdam, the Netherlands (nr MEC 221.520/2002/262; date of approval: 22 July 2003, and MEC-2005-057, date of approval: 14 February 2005). All patients gave written informed consent to use their tissue for research purposes.

Primary Cell Cultures. Primary glioma cell cultures were established as described previously.³⁹ Briefly, fresh tumor tissue was collected as solid pieces of resected tumor tissue or Cavitron Ultrasonic Surgical Aspirator (CUSA) tissue fragments from the operating theater, and processed within 4 h after resection. Tissue was divided into two parts, half of the sample was snap-frozen in liquid nitrogen, and subsequently stored at $-80\text{ }^{\circ}\text{C}$, and the other half was used for cell culture establishment. Tissue was mechanically dissociated with a scalpel and then enzymatically dissociated with collagenase A and DNase. Red blood cells were removed with an erythrocyte lysis buffer. All cell cultures were started in serum-free medium (DMEM/F12, 11320-074) with the following supplements: 1% penicillin/streptomycin (15140-122), 1× B27 (12587-010), 20 ng/mL basic fibroblast growth factor (bFGF,

PHG0263), 20 ng/mL epidermal growth factor (EGF, PHG0313), and 5 $\mu\text{g/mL}$ heparin (A16198). Samples were cultured in suspension for 5–7 days and then transferred to culture flasks coated with 1:100 diluted Cultrex PathClear Reduced Growth Factor BME (R&D Systems) for adherent culture. All cultures were grown at 37 °C in a humidified incubator with 5% CO₂. Cultures were detached with Accutase (Invitrogen) when 90% confluence was reached and passaged, typically 1:3.

Sample Preparation. Cryosections of 5 μm were cut at –20 °C, stained with hematoxylin and eosin (H&E), and reviewed by a certified pathologist to determine the tumor cell percentage. Only samples with a minimum of 50% tumor cell content were included for analysis. For the proteomics analysis, consecutive 10 μm sections were cut corresponding to a total of approximately one square centimeter of tissue surface. The sections were stored at –80 °C until H&E staining and trypsin digestion. For the primary cell cultures, the cells from one 90% confluent T75 culture flask were dissociated with Accutase, centrifuged in an Eppendorf tube, washed with cold phosphate-buffered saline, and subsequently stored at –80 °C until digestion. For digestion, 100 μL of lysis buffer containing 7.5 mM dithiothreitol (DTT) with 5% (w/v) sodium deoxycholate (SDC) was added to each sample. The samples were then disrupted by a sonication probe for 2 min at 70% amplitude (Branson, Ultrasonic, Danbury, CT); afterward, the samples were incubated in a Thermomixer for 10 min at 80 °C (Eppendorf Thermomixer comfort). Then, 5 μL of 100 mM DTT was added followed by a 20 min incubation at 60 °C. Next, 5 μL of 375 mM IAA (iodoacetamide) was added and the samples were incubated protected from light at room temperature. Then, 900 μL of –20 °C acetone was added followed by centrifugation with an Eppendorf centrifuge at a maximum speed for 10 min at 4 °C. The supernatant was removed and 80 μL of digestion buffer was added containing 50 mM triethylammonium bicarbonate buffer (TEAB) with 5% v/v acetonitrile and 0.5% w/v SDC, the pellet was dissolved, and 2 μg of trypsin (1:100 ratio; Mass Spectrometry Grade, Promega Corporation) was added to each sample. The samples were then incubated overnight followed by acidification with 80 μL of 1% v/v trifluoroacetic acid (TFA). The samples were centrifuged at 20 200 RCF for 10 min at 4 °C, and then the supernatant was transferred to another tube. The samples were diluted 10-fold with 0.1% v/v TFA and measured on a nano-LC system (UltiMate 3000 RSLCnano system, Thermo Fisher Scientific, Germering, Germany). The total protein content was calculated based on the intensity of the absorbance at 214 nm over the span of a 15 min gradient. The samples were normalized based on this integrated UV–vis intensity value and then stored at 4 °C until further use. A Pierce Quantitative Colorimetric Peptide Assay (Thermo Scientific, Pierce) was performed according to the manufacturer's recommendation to determine the total amount of peptides in the samples.

Targeted MS Measurements Metabolic Enzymes. Of all samples, 300 ng of digested protein was measured either on an Orbitrap Eclipse Tribrid MS or an Orbitrap Fusion Lumos Tribrid MS (Thermo Fisher Scientific, San Jose, CA). A cross-validation was performed between both systems to exclude a system bias. In both cases, the Orbitrap MS was set up with a nano-LC system (Ultimate 3000, Thermo Fisher Scientific, Germering, Germany) equipped with a reversed-phase column (PepMap C18, 75 μm internal diameter, 25 cm in length, 2 μm

particle size, and 100 Å pore size). A linear 90 min gradient was used with 0.08% v/v formic acid in 80% v/v acetonitrile as an organic solvent, starting at 4% organic solvent, and increasing to 38% organic solvent with a flow of 300 nL/min. The MS parameters applied were similar for both systems. The ion source was set to nanospray ionization with a static spray voltage of 1800 V. The ion transfer tube temperature was set to 275 °C. The resolving power of the Orbitrap was 60 000, and the scan range mode was set to automatic. The automatic gain control (AGC) was set to 50 000, and the injection time was 118 ms. The isolation window was set to 0.6 m/z ; as the fragmentation method, higher-energy collisional dissociation (HCD) was used with a normalized collision energy (NCE) of 28%. In total, 120 peptide targets were selected corresponding to 64 proteins (see Supporting Information Table S2). Of each peptide, the retention time was determined based on a pilot run. Subsequently, all samples were analyzed with a retention time window set to 5 min in a scheduled method of 90 min.

A separate PRM measurement was carried out targeting peptides specific for IDH1 to determine the IDH1 status of the tissue samples and primary cell culture samples (Table S3). Five different heavy labeled peptides (AQUA QuantPro, Thermo Scientific) were used by the addition of 20 μL of peptide mix containing 0.2 fmol of each peptide to 20 μL sample. For this analysis, a short 30 min linear gradient was used. For the cultures, all parameters were kept the same as during the PRM measurements for the metabolic enzymes. For the analysis on tissue, the Orbitrap Eclipse Tribrid MS was used with a FAIMS device to gain a higher sensitivity. Different FAIMS compensation voltages (CV) were tested for these peptides in a pilot experiment, and the CV that gave the highest signal for the peptide was used for the sample measurement. The ion source was set to nanospray ionization with a static spray voltage of 2200 V. The ion transfer tube temperature was set to 305 °C. The resolving power of the Orbitrap was set to 120 000, and the injection time was set to 246 ms for the IDH1 mutant (mut) peptides and one IDH1 wild-type (wt) peptide. For the remaining peptides, the resolving power was set to 60 000 and the injection time was set to 118 ms (see Supporting Information Table S3). All of the other parameters were kept the same as the PRM measurements for the metabolic enzymes.

Whole Proteome MS Measurements. The primary cell cultures were analyzed by a data-dependent acquisition (DDA) method. The Orbitrap Eclipse was used in combination with the nano-LC system described above, using the same 90 min gradient. The MS system was used with a FAIMS device (FAIMS Pro Interface, Thermo Fisher Scientific). The compensation voltages (CVs) of the device were set to –45, –60, –75, and –90 with a cycle time of 1 s.⁴⁰ A static spray voltage of 2200 V was used, and the ion transfer tube temperature was set to 305 °C. For the parent scan, the resolving power of the Orbitrap was 120 000 and a scan range of 375–1500 m/z was applied. The AGC was 400,000, and the injection time was 50 ms. The isolation window was set to 1.6 m/z , HCD was used with an NCE of 30%, and the ion trap was operated in rapid scanning mode for the MS/MS scans with an AGC of 10 000 and an injection time of 35 ms.

Data Processing Targeted MS. The PRM data were analyzed with Skyline-daily (20.1.1.32, MacCoss Lab, Department of Genome Sciences, Seattle, WA). For each targeted mass, multiple transitions were selected. The peak areas were integrated based on fragment mass, expected mass error, and

retention time. The area under the curve for each transition was exported to Excel and summed for each peptide. A correlation plot was made for the peptides from the same protein to validate whether these peptides represent the abundance of the protein accurately. The abundance values of all proteins were further analyzed in Perseus (version 1.6.1.2, Computational Systems Biochemistry, Martinsried, Germany). The samples were divided into two groups based on the IDH1 status, and each value was transformed with a log₂ factor; subsequently, a *t*-test and randomization of the data were performed to determine a false discovery rate (FDR). The data were used to generate volcano plots.

Data Processing Whole Proteome Analysis. The raw files generated by Thermo Xcalibur were analyzed in parallel by Proteome Discoverer (1.4, Thermo Scientific, Waltham, MA) and Mascot (version 2.3.02, Matrix Science, Inc., Chicago, IL) with the uniprot_sprot_HUMAN_v151112 database. The modification parameters were set to carbamidomethylation as a fixed modification on cysteine, oxidation as a variable modification on methionine, and carbamidomethylation as a variable modification on N-terminal amino acids. Trypsin was selected as a digestive enzyme. The fragment tolerance was set to 0.50 Da, the parent tolerance was set to 10.0 ppm, and the maximum amount of miss cleavages was set to 2. The generated files were then loaded into Scaffold (version 4.10.0, Proteome Software, Inc., Portland, OR) and combined into a single biosample containing both the Proteome Discoverer file and Mascot file. Filter criteria for protein identification were set to a protein threshold and peptide threshold of 1.0% FDR with a minimum of two peptides. The data were normalized based on total spectral counts, resulting in a quantitative value for all identified protein groups, which were further analyzed in Perseus. The samples were divided into two groups based on the IDH1 status and each value was transformed with a log₂ factor. Proteins were filtered for having an abundance higher than 0 for at least 70% of the samples in one group, missing values were then imputed from the normal distribution. Statistical analyses were performed (*t*-test and randomization of the data to determine FDR), and the data were normalized to a z-score for hierarchical clustering.

■ ASSOCIATED CONTENT

SI Supporting Information

The Supporting Information is available free of charge at <https://pubs.acs.org/doi/10.1021/acsomega.1c06121>.

Correlation plot of the current study's log₂ fold change compared to the previous study's log₂ fold change (Figure S1); additional volcano plot analysis comparing low-grade with high-grade IDH1 mutant gliomas (Figure S2); correlation plot of the tissue subset log₂ fold change compared to the complete tissue set log₂ fold change (Figure S3); correlation of the primary culture set log₂ fold changes and the tissue set (Figure S4); correlation of the xenograft log₂ fold changes compared to the complete tissue set log₂ fold changes (Figure S5); additional tissue and culture information (Table S1); list of metabolic enzymes with precursor masses (Table S2); list of peptides measured for the IDH1 status determination (Table S3); results of volcano plot analysis comparing IDH1 wt with IDH1 mut glioma tissues (Table S4); results of volcano plot analysis

comparing the IDH1 wt and IDH1 mut samples of the tissue subset (Table S5); results of volcano plot analysis comparing the IDH1 wt and IDH1 mut samples of the culture sample set (Table S6); and comparison of the fold changes observed between IDH1 mut and IDH1 wt tissues and the fold changes observed between IDH1 mut and IDH1 wt xenografts (Table S7) (PDF)

■ AUTHOR INFORMATION

Corresponding Author

Theo M. Luider – *Laboratories of Neuro-Oncology/Clinical and Cancer Proteomics, Department of Neurology, Erasmus MC, Rotterdam, 3000 CA Rotterdam, The Netherlands;*
orcid.org/0000-0003-1962-561X; Phone: +31 10 703 80 69; Email: t.luider@erasmusmc.nl

Authors

Lennard J. M. Dekker – *Laboratories of Neuro-Oncology/Clinical and Cancer Proteomics, Department of Neurology, Erasmus MC, Rotterdam, 3000 CA Rotterdam, The Netherlands*

Cassandra Verheul – *Department of Neurosurgery, Erasmus MC, Rotterdam, 3000 CA Rotterdam, The Netherlands*

Nicky Wensveen – *Laboratories of Neuro-Oncology/Clinical and Cancer Proteomics, Department of Neurology, Erasmus MC, Rotterdam, 3000 CA Rotterdam, The Netherlands*

William Leenders – *Department of Biochemistry, Radboud Institute for Molecular Life Sciences, 6500 HB Nijmegen, The Netherlands;* orcid.org/0000-0003-0066-220X

Martine L. M. Lamfers – *Department of Neurosurgery, Erasmus MC, Rotterdam, 3000 CA Rotterdam, The Netherlands*

Sieger Leenstra – *Department of Neurosurgery, Erasmus MC, Rotterdam, 3000 CA Rotterdam, The Netherlands*

Complete contact information is available at:

<https://pubs.acs.org/10.1021/acsomega.1c06121>

Author Contributions

L.D., T.L., and M.L. contributed to the study design. C.V., N.W., and L.D. performed sample collection and selection. Clinical information was obtained from C.V. L.D., N.W., C.V., and W.L. carried out the experiments. L.D., N.W., C.V., and W.L. performed data analyses. L.D., C.V., N.W., W.L., M.L., S.L., and T.L. contributed to discussion and writing. All authors read and approved the final manuscript.

Notes

The authors declare no competing financial interest. The mass spectrometry proteomics data have been deposited to the ProteomeXchange Consortium via the PRIDE partner repository with the data set identifier PXD024009, 10.6019/PXD024009, and PXD024019.

■ ACKNOWLEDGMENTS

This research was (partially) funded by NWO, project 184.034.019. C.V. was financially supported by STOPPhersentumoren.

■ LIST OF ABBREVIATIONS

IDH 1/2 isocitrate dehydrogenase 1 and 2
 α -KG α -ketoglutarate
TCA tricarboxylic acid
EGCG catechol epigallocatechin gallate

AA	anaplastic astrocytomas
CUSA	cavitron ultrasonic surgical aspirator
TFA	trifluoroacetic acid
DTT	dithiothreitol
SDC	sodium deoxycholate
IAA	iodoacetamide
NCE	normalized collision energy
AGC	automatic gain control
DDA	data-dependent acquisition

REFERENCES

- Ostrom, Q. T.; Gittleman, H.; Truitt, G.; Boscia, A.; Kruchko, C.; Barnholtz-Sloan, J. S. CBTRUS Statistical Report: Primary Brain and Other Central Nervous System Tumors Diagnosed in the United States in 2011–2015. *Neuro-Oncology* **2018**, *20*, iv1–iv86.
- Hartmann, C.; Meyer, J.; Balss, J.; Capper, D.; Mueller, W.; Christians, A.; Felsberg, J.; Wolter, M.; Mawrin, C.; Wick, W.; Weller, M.; Herold-Mende, C.; Unterberg, A.; Jeuken, J. W. M.; Wesseling, P.; Reifenberger, G.; von Deimling, A. Type and frequency of IDH1 and IDH2 mutations are related to astrocytic and oligodendroglial differentiation and age: a study of 1,010 diffuse gliomas. *Acta Neuropathol.* **2009**, *118*, 469–474.
- Yan, H.; Parsons, D. W.; Jin, G.; McLendon, R.; Rasheed, B. A.; Yuan, W.; Kos, I.; Batinic-Haberle, I.; Jones, S.; Riggins, G. J.; Friedman, H.; Friedman, A.; Reardon, D.; Herndon, J.; Kinzler, K. W.; Velculescu, V. E.; Vogelstein, B.; Bigner, D. D. IDH1 and IDH2 mutations in gliomas. *N. Engl. J. Med.* **2009**, *360*, 765–773.
- Dang, L.; White, D. W.; Gross, S.; Bennett, B. D.; Bittinger, M. A.; Driggers, E. M.; Fantin, V. R.; Jang, H. G.; Jin, S.; Keenan, M. C.; Marks, K. M.; Prins, R. M.; Ward, P. S.; Yen, K. E.; Liao, L. M.; Rabinowitz, J. D.; Cantley, L. C.; Thompson, C. B.; Vander Heiden, M. G.; Su, S. M. Cancer-associated IDH1 mutations produce 2-hydroxyglutarate. *Nature* **2009**, *462*, 739–744.
- Fack, F.; Tardito, S.; Hochart, G.; Oudin, A.; Zheng, L.; Fritah, S.; Golebiewska, A.; Nazarov, P. V.; Bernard, A.; Hau, A. C.; Keunen, O.; Leenders, W.; Lund-Johansen, M.; Stauber, J.; Gottlieb, E.; Bjerkvig, R.; Niclou, S. P. Altered metabolic landscape in IDH-mutant gliomas affects phospholipid, energy, and oxidative stress pathways. *EMBO Mol. Med.* **2017**, *9*, 1681–1695.
- Dekker, L. J. M.; Wu, S.; Jurriens, C.; Mustafa, D. A. N.; Grevers, F.; Burgers, P. C.; Sillevius Smitt, P. A. E.; Kros, J. M.; Luider, T. M. Metabolic changes related to the IDH1 mutation in gliomas preserve TCA-cycle activity: An investigation at the protein level. *FASEB J.* **2020**, *34*, 3646–3657.
- Lenting, K.; Khurshed, M.; Peeters, T. H.; van den Heuvel, C.; van Lith, S. A. M.; de Bitter, T.; Hendriks, W.; Span, P. N.; Molenaar, R. J.; Botman, D.; Verrijp, K.; Heerschap, A.; Ter Laan, M.; Kusters, B.; van Ewijk, A.; Huynen, M. A.; van Noorden, C. J. F.; Leenders, W. P. J. Isocitrate dehydrogenase 1-mutated human gliomas depend on lactate and glutamate to alleviate metabolic stress. *FASEB J.* **2019**, *33*, 557–571.
- Zhou, L.; Wang, Z.; Hu, C.; Zhang, C.; Kovatcheva-Datchary, P.; Yu, D.; Liu, S.; Ren, F.; Wang, X.; Li, Y.; Hou, X.; Piao, H.; Lu, X.; Zhang, Y.; Xu, G. Integrated Metabolomics and Lipidomics Analyses Reveal Metabolic Reprogramming in Human Glioma with IDH1 Mutation. *J. Proteome Res.* **2019**, *18*, 960–969.
- Mustafa, D. A. N.; Swagemakers, S. M.; Buise, L.; van der Spek, P. J.; Kros, J. M. Metabolic alterations due to IDH1 mutation in glioma: opening for therapeutic opportunities? *Acta Neuropathol. Commun.* **2014**, *2*, No. 6.
- Fack, F.; Tardito, S.; Hochart, G.; Oudin, A.; Zheng, L.; Fritah, S.; Golebiewska, A.; Nazarov, P. V.; Bernard, A.; Hau, A. C.; Keunen, O.; Leenders, W.; Lund-Johansen, M.; Stauber, J.; Gottlieb, E.; Bjerkvig, R.; Niclou, S. P. Altered metabolic landscape in IDH-mutant gliomas affects phospholipid, energy, and oxidative stress pathways. *EMBO Mol. Med.* **2017**, *9*, 1681–1695.
- Khurshed, M.; Lenting, K.; Molenaar, R. J.; Leenders, W. P.; Noorden, C. J. v. Abstract 431: IDH1-mutated gliomas rely on anaplerosis of glutamate and lactate whereas IDH1 wild-type gliomas rely on glycolysis and acetate anaplerosis. *Cancer Res.* **2017**, *77*, No. 431.
- Grassian, A. R.; Parker, S. J.; Davidson, S. M.; Divakaruni, A. S.; Green, C. R.; Zhang, X.; Slocum, K. L.; Pu, M.; Lin, F.; Vickers, C.; Joud-Caldwell, C.; Chung, F.; Yin, H.; Handly, E. D.; Straub, C.; Growney, J. D.; Vander Heiden, M. G.; Murphy, A. N.; Pagliarini, R.; Metallo, C. M. IDH1 Mutations Alter Citric Acid Cycle Metabolism and Increase Dependence on Oxidative Mitochondrial Metabolism. *Cancer Res.* **2014**, *74*, 3317–3331.
- Peeters, T. H.; Lenting, K.; Breukels, V.; van Lith, S. A. M.; van den Heuvel, C. N. A. M.; Molenaar, R.; van Rooij, A.; Wevers, R.; Span, P. N.; Heerschap, A.; Leenders, W. P. J. Isocitrate dehydrogenase 1-mutated cancers are sensitive to the green tea polyphenol epigallocatechin-3-gallate. *Cancer Metab.* **2019**, *7*, No. 4.
- Verheul, C.; Ntafoulis, I.; Kers, T. V.; Hoogstrate, Y.; Mastroberardino, P. G.; Barnhoorn, S.; Payán-Gómez, C.; Tching Chi Yen, R.; Struys, E. A.; Koolen, S. L. W.; Dirven, C. M. F.; Leenstra, S.; French, P. J.; Lamfers, M. L. M. Generation, characterization, and drug sensitivities of 12 patient-derived IDH1-mutant glioma cell cultures. *Neuro-Oncology Adv.* **2021**, *3*, No. vdb103.
- Berghauser Pont, L. M.; Balvers, R. K.; Kloezeman, J. J.; Nowicki, M. O.; van den Bossche, W.; Kremer, A.; Wakimoto, H.; van den Hoogen, B. G.; Leenstra, S.; Dirven, C. M.; Chiocca, E. A.; Lawler, S. E.; Lamfers, M. L. In vitro screening of clinical drugs identifies sensitizers of oncolytic viral therapy in glioblastoma stem-like cells. *Gene Ther.* **2015**, *22*, 947–959.
- Demidenko, E. The p-Value You Can't Buy. *Am. Stat.* **2016**, *70*, 33–38.
- Jones, L. E.; Hilz, S.; Grimmer, M. R.; Mazor, T.; Najac, C.; Mukherjee, J.; McKinney, A.; Chow, T.; Pieper, R. O.; Ronen, S. M.; Chang, S. M.; Phillips, J. J.; Costello, J. F. Patient-derived cells from recurrent tumors that model the evolution of IDH-mutant glioma. *Neuro-Oncol. Adv.* **2020**, *2*, No. vdaa088.
- Kelly, J. J.; Blough, M. D.; Stechishin, O. D.; Chan, J. A.; Beauchamp, D.; Perizzolo, M.; Demetrick, D. J.; Steele, L.; Auer, R. N.; Hader, W. J.; Westgate, M.; Parney, I. F.; Jenkins, R.; Cairncross, J. G.; Weiss, S. Oligodendroglioma cell lines containing t(1;19)-(q10;p10). *Neuro-Oncology* **2010**, *12*, 745–755.
- Laks, D. R.; Crisman, T. J.; Shih, M. Y. S.; Mottahedeh, J.; Gao, F.; Sperry, J.; Garrett, M. C.; Yong, W. H.; Cloughesy, T. F.; Liao, L. M.; Lai, A.; Coppola, G.; Kornblum, H. I. Large-scale assessment of the gliomasphere model system. *Neuro-Oncology* **2016**, *18*, 1367–1378.
- Luchman, H. A.; Stechishin, O. D.; Dang, N. H.; Blough, M. D.; Chesnelong, C.; Kelly, J. J.; Nguyen, S. A.; Chan, J. A.; Weljie, A. M.; Cairncross, J. G.; Weiss, S. An in vivo patient-derived model of endogenous IDH1-mutant glioma. *Neuro-Oncology* **2012**, *14*, 184–191.
- Lesur, A.; Ancheva, L.; Kim, Y. J.; Berchem, G.; van Oostrum, J.; Domon, B. Screening protein isoforms predictive for cancer using immunoaffinity capture and fast LC-MS in PRM mode. *Proteomics* **2015**, *9*, 695–705.
- Zenedpour, L.; Dekker, L. J. M.; van Sten-van't Hoff, J. J. M.; Burgers, P. C.; ten Hacken, N. H. T.; Luider, T. M. Neoantigens in Chronic Obstructive Pulmonary Disease and Lung Cancer: A Point of View. *Proteomics* **2019**, *13*, No. 1800093.
- Perrin, S. L.; Samuel, M. S.; Koszyca, B.; Brown, M. P.; Ebert, L. M.; Oksdath, M.; Gomez, G. A. Glioblastoma heterogeneity and the tumour microenvironment: implications for preclinical research and development of new treatments. *Biochem. Soc. Trans.* **2019**, *47*, 625–638.
- Lenting, K.; Verhaak, R.; Ter Laan, M.; Wesseling, P.; Leenders, W. Glioma: experimental models and reality. *Acta Neuropathol.* **2017**, *133*, 263–282.
- Verjans, E. T.; Doijen, J.; Luyten, W.; Landuyt, B.; Schoofs, L. Three-dimensional cell culture models for anticancer drug screening: Worth the effort? *J. Cell. Physiol.* **2018**, *233*, 2993–3003.

(26) Biancur, D. E.; Paulo, J. A.; Malachowska, B.; Quiles Del Rey, M.; Sousa, C. M.; Wang, X.; Sohn, A. S. W.; Chu, G. C.; Gygi, S. P.; Harper, J. W.; Fendler, W.; Mancias, J. D.; Kimmelman, A. C. Compensatory metabolic networks in pancreatic cancers upon perturbation of glutamine metabolism. *Nat. Commun.* **2017**, *8*, No. 15965.

(27) Davidson, S. M.; Papagiannakopoulos, T.; Olenchock, B. A.; Heyman, J. E.; Keibler, M. A.; Luengo, A.; Bauer, M. R.; Jha, A. K.; O'Brien, J. P.; Pierce, K. A.; Gui, D. Y.; Sullivan, L. B.; Wasylenko, T. M.; Subbaraj, L.; Chin, C. R.; Stephanopoulos, G.; Mott, B. T.; Jacks, T.; Clish, C. B.; Vander Heiden, M. G. Environment Impacts the Metabolic Dependencies of Ras-Driven Non-Small Cell Lung Cancer. *Cell Metab.* **2016**, *23*, 517–528.

(28) Vande Voorde, J.; Ackermann, T.; Pftzer, N.; Sumpton, D.; Mackay, G.; Kalna, G.; Nixon, C.; Blyth, K.; Gottlieb, E.; Tardito, S. Improving the metabolic fidelity of cancer models with a physiological cell culture medium. *Sci. Adv.* **2019**, *5*, No. eaau7314.

(29) Leen, W. G.; Willemsen, M. A.; Wevers, R. A.; Verbeek, M. M. Cerebrospinal fluid glucose and lactate: age-specific reference values and implications for clinical practice. *PLoS One* **2012**, *7*, No. e42745.

(30) Alves, A. L. V.; Gomes, I. N. F.; Carloni, A. C.; Rosa, M. N.; Da Silva, L. S.; Evangelista, A. F.; Reis, R. M.; Silva, V. A. O. Role of glioblastoma stem cells in cancer therapeutic resistance: a perspective on antineoplastic agents from natural sources and chemical derivatives. *Stem Cell Res. Ther.* **2021**, *12*, 1–22.

(31) Lee, J.; Kotliarova, S.; Kotliarov, Y.; Li, A.; Su, Q.; Donin, N. M.; Pastorino, S.; Purow, B. W.; Christopher, N.; Zhang, W.; Park, J. K.; Fine, H. A. Tumor stem cells derived from glioblastomas cultured in bFGF and EGF more closely mirror the phenotype and genotype of primary tumors than do serum-cultured cell lines. *Cancer Cell* **2006**, *9*, 391–403.

(32) Bralten, L. B.; Kloosterhof, N. K.; Balvers, R.; Sacchetti, A.; Lapre, L.; Lamfers, M.; Leenstra, S.; de Jonge, H.; Kros, J. M.; Jansen, E. E.; Struys, E. A.; Jakobs, C.; Salomons, G. S.; Diks, S. H.; Peppelenbosch, M.; Kremer, A.; Hoogenraad, C. C.; Smitt, P. A.; French, P. J. IDH1 R132H decreases proliferation of glioma cell lines in vitro and in vivo. *Ann. Neurol.* **2011**, *69*, 455–463.

(33) Parker, J. J.; Lizarraga, M.; Waziri, A.; Foshay, K. M. A Human Glioblastoma Organotypic Slice Culture Model for Study of Tumor Cell Migration and Patient-specific Effects of Anti-Invasive Drugs. *J. Visualized Exp.* **2017**, No. e53557.

(34) Hamer Philip, C. D. W.; Jonker, A.; Leenstra, S.; Ruijter, J. M.; Noorden, C. J. F. V. Quantification of Viability in Organotypic Multicellular Spheroids of Human Malignant Glioma using Lactate Dehydrogenase Activity: A Rapid and Reliable Automated Assay. *J. Histochem. Cytochem.* **2005**, *53*, 23–34.

(35) Ayuso, J. M.; Monge, R.; Martínez-González, A.; Virumbrales-Muñoz, M.; Llamazares, G. A.; Berganzo, J.; Hernández-Lain, A.; Santolaria, J.; Doblaré, M.; Hubert, C.; Rich, J. N.; Sánchez-Gómez, P.; Pérez-García, V. M.; Ochoa, I.; Fernández, L. J. Glioblastoma on a microfluidic chip: Generating pseudopalisades and enhancing aggressiveness through blood vessel obstruction events. *Neuro-Oncology* **2017**, *27*, No. now230.

(36) Jacob, F.; Salinas, R. D.; Zhang, D. Y.; Nguyen, P. T. T.; Schnoll, J. G.; Wong, S. Z. H.; Thokala, R.; Sheikh, S.; Saxena, D.; Prokop, S.; Liu, D.-A.; Qian, X.; Petrov, D.; Lucas, T.; Chen, H. I.; Dorsey, J. F.; Christian, K. M.; Binder, Z. A.; Nasrallah, M.; Brem, S.; O'Rourke, D. M.; Ming, G.-L.; Song, H. A Patient-Derived Glioblastoma Organoid Model and Biobank Recapitulates Inter- and Intra-tumoral Heterogeneity. *Cell* **2020**, *180*, 188–204.e22.

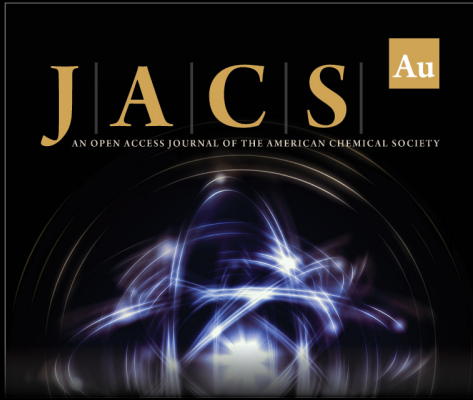
(37) Golebiewska, A.; Hau, A. C.; Oudin, A.; Stieber, D.; Yabo, Y. A.; Baus, V.; Barthelemy, V.; Klein, E.; Bougnaud, S.; Keunen, O.; Wantz, M.; Michelucci, A.; Neirinckx, V.; Muller, A.; Kaoma, T.; Nazarov, P. V.; Azuaje, F.; De Falco, A.; Flies, B.; Richart, L.; Poovathingal, S.; Arns, T.; Grzyb, K.; Mock, A.; Herold-Mende, C.; Steino, A.; Brown, D.; May, P.; Miletic, H.; Malta, T. M.; Noushmehr, H.; Kwon, Y. J.; Jahn, W.; Klink, B.; Tanner, G.; Stead, L. F.; Mittelbronn, M.; Skupin, A.; Hertel, F.; Bjerkvig, R.; Niclou, S. P. Patient-derived organoids and orthotopic xenografts of primary and

recurrent gliomas represent relevant patient avatars for precision oncology. *Acta Neuropathol.* **2020**, *140*, 919–949.

(38) Louis, D. N.; Perry, A.; Reifenberger, G.; von Deimling, A.; Figarella-Branger, D.; Cavenee, W. K.; Ohgaki, H.; Wiestler, O. D.; Kleihues, P.; Ellison, D. W. The 2016 World Health Organization Classification of Tumors of the Central Nervous System: a summary. *Acta Neuropathol.* **2016**, *131*, 803–820.


(39) Balvers, R. K.; Kleijn, A.; Kloezeman, J. J.; French, P. J.; Kremer, A.; van den Bent, M. J.; Dirven, C. M.; Leenstra, S.; Lamfers, M. L. Serum-free culture success of glial tumors is related to specific molecular profiles and expression of extracellular matrix-associated gene modules. *Neuro-Oncology* **2013**, *15*, 1684–1695.


(40) Hebert, A. S.; Prasad, S.; Belford, M. W.; Bailey, D. J.; McAlister, G. C.; Abbatiello, S. E.; Huguet, R.; Wouters, E. R.; Dunyach, J. J.; Brademan, D. R.; Westphall, M. S.; Coon, J. J. Comprehensive Single-Shot Proteomics with FAIMS on a Hybrid Orbitrap Mass Spectrometer. *Anal. Chem.* **2018**, *90*, 9529–9537.



JACS Au
AN OPEN ACCESS JOURNAL OF THE AMERICAN CHEMICAL SOCIETY

Editor-in-Chief
Prof. Christopher W. Jones
Georgia Institute of Technology, USA

Open for Submissions 

pubs.acs.org/jacsau  ACS Publications
Most Trusted. Most Cited. Most Read.